ISSN (Print) 1226-1750
ISSN (Online) 2233-6656
Journal of Magnetics 19(4), 411-417 (2014) http://dx.doi.org/10.4283/JMAG.2014.19.4.411

Analysis and Design of a Novel-Shape Permanent Magnet Synchronous Motor for Minimization of Torque Ripple and Iron Loss

Jin-Hong Kim[1,3], Jung-Moo Seo[1,2]*, Hyun-Kyo Jung[2], and Chung-Yuen Won[3]

[1]*Korea Electronics Technology Institute, Bucheon 420-733, Korea*
[2]*Dept. of Electrical and Computer Engineering, Seoul National University, Seoul 151-742, Korea*
[3]*Dept. of Electrical and Computer Engineering, Sungkyunkwan University, Suwon 440-746, Korea*

(Received 28 October 2014, Received in final form 12 December 2014, Accepted 16 December 2014)

This paper presents the shape optimization of a permanent magnet synchronous motor to reduce the torque ripple and iron loss. Specifically, the harmonics of the electromotive force and cogging torque are decreased by adjusting the permanent magnet arrangement and non-uniform air gap length. In addition, an additional flux path along the *q*-axis is proposed with a unique rotor shape to increase the *q*-axis inductance and reluctance torque. The improvement in the performance of the proposed model is verified with simulated and experimental results.

Keywords : cogging torque, permanent magnet synchronous motor, shape optimization, torque ripple, THD of the electromotive force

1. Introduction

Parasitic torque pulsation, which is one of the main disadvantages of a permanent magnet synchronous motor (PMSM), can cause vibration and acoustic noise. The torque ripple is affected by the sinusoidal character of the back electromotive force (EMF) and input current waveforms, and the magnitude of the cogging torque [1-6]. Therefore, it is necessary to minimize the harmonic components of the EMF and cogging torque to improve the performance during the motor design stage. Furthermore, the reduced total harmonic distortion (THD) of the EMF leads to a decrease in the iron loss developed from the harmonics of the air gap flux density because the THD of the EMF is directly related to the air gap flux density distribution [7-10].

This paper presents the optimal design for the rotor core of a PMSM to minimize the torque ripple and iron loss. By changing the configuration of the PM inside the rotor core and applying a non-uniform air gap length outside the rotor core, a sinusoidal distribution is obtained for the air gap flux density. The sinusoidal flux distribution decreases the cogging torque and harmonic components of the flux linkage and back EMF, thereby allowing for a reduction in the torque ripple and iron loss. Furthermore, an additional q-axis flux path is applied to the rotor to increase the reluctance torque according to the saliency ratio, which increases the output power and efficiency of the motor.

2. Design and Analysis for Torque Ripple and Iron Loss Reduction

2.1. Initial Model

Fig. 1 and Table 1 present the basic shape and specifications, respectively, of the primary designed PMSM with

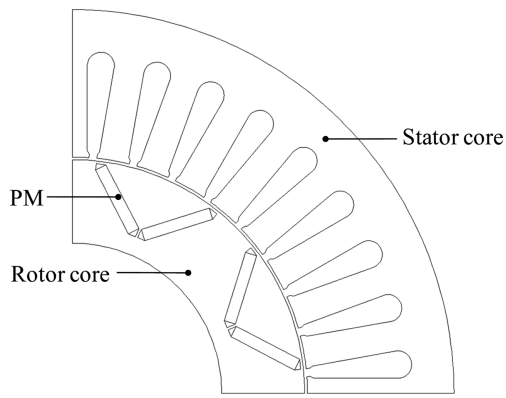

Fig. 1. Designed PMSM with a V-shaped PM.

©The Korean Magnetics Society. All rights reserved.
*Corresponding author: Tel: +82-32-621-2852
Fax: +82-32-621-2855, e-mail: sjm@keti.re.kr

© 2014 Journal of Magnetics

Table 1. Specifications of the Designed Motor.

Parameter	Value	Units
number of poles/slots	8/36	–
rated power	20	kW
rated speed	4,000	rpm
stator core diameter	230	mm
active length	115	mm
residual flux density of the PM	1.25	T

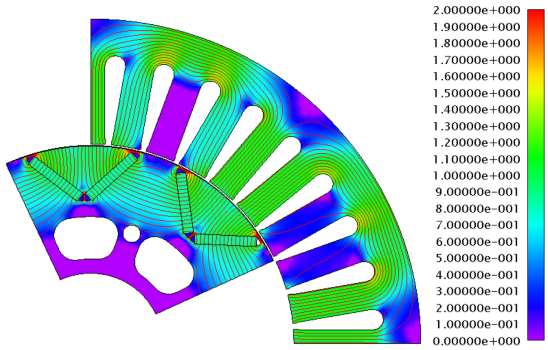

(a)

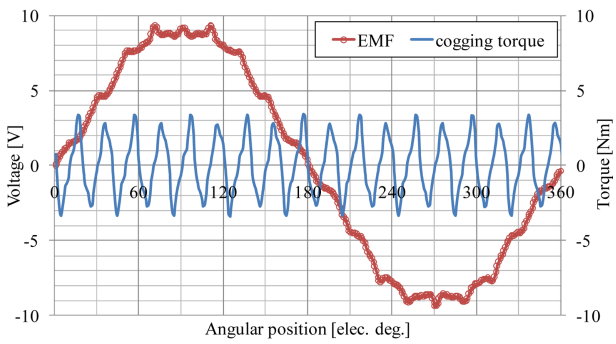

(b)

Fig. 2. (Color online) No-load analysis results of the designed motor at 1,000 rpm. (a) Magnetic flux density. (b) EMF and cogging torque.

an output power of 20 kW. The motor is an interior permanent magnet synchronous motor (IPMSM) having 8 poles/36 slots with a distributed winding, and the PMs are arranged in V-shape for flux concentration. Fig. 2 shows the no-load analysis results of the designed motor. The maximum flux densities of the stator teeth and yoke are calculated to be less than 1.2 T. In addition, the back EMF at a rotational speed of 1,000 rpm is approximately 9.0 V_{rms}, and the cogging torque is 3.3 $Nm_{0\text{-}p}$. On the basis of the given structure, the *d*- and *q*-axis inductances are calculated with respect to the input current variations, and the output torque is determined by the calculated inductance and current as follows [11, 12]:

$$T = P_n\{\psi_a i_{od} + (L_d - L_q) i_{od} i_{oq}\}, \quad (1)$$

where P_n is the number of pole pairs, and Ψ_a is the flux linkage by the permanent magnet. L_d and L_q and i_{od} and i_{oq} are *d*- and *q*-axis armature self inductances and load currents, respectively.

2.2. Improved Model

The initially designed motor satisfies the required output characteristics; however, the THD of the EMF and the cogging torque are much higher considering the sinusoidal current and rated torque. The THD is measurement of the harmonic distortion present and is defined as the ratio of the sum of the powers of all harmonic components to the power of the fundamental frequency. A lower THD of the EMF means that the waveform of the EMF is similar to a sinusoidal waveform. The cogging torque is developed from variations in the air gap magnetic energy; the extent of the variation between the stator teeth and the rotor magnets determines the magnitude of the cogging torque. For the PMSM, the sinusoidal character of the back EMF and current waveforms and the cogging torque are related to the torque ripple. An increased torque ripple lowers the performance of the motor owing to noise, vibration, and hard starting [13-15]. Therefore, in terms of motor design, optimal design of the rotor and stator is required to reduce the THD of the EMF and the cogging torque. In addition, the sinusoidal EMF is directly connected to the THD of the air gap flux density, and the reduced THD of the EMF means lower iron loss, which is generated from the harmonics of the air gap flux density.

In this study, the inside and outside shapes of the rotor core are changed to improve the motor performance without changing the stator core of the initial model. Fig. 3 shows two design variables to decrease the THD of the EMF and the cogging torque. One is the pole arc to pole

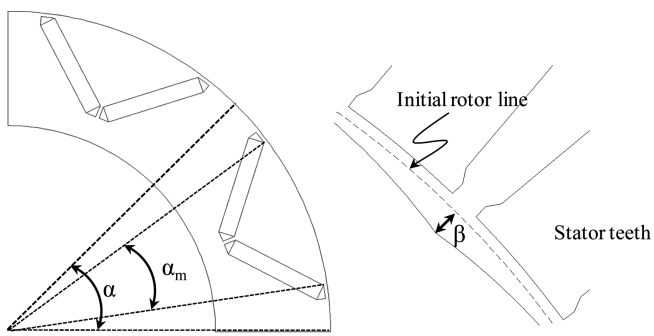

(a) (b)

Fig. 3. Design variables of the rotor core. (a) Pole arc to pole pitch ratio (α_m/α). (b) Air gap length for the eccentric rotor surface (β).

pitch ratio (α_m/α), and the other is the air gap length for the eccentric rotor surface (β). A fundamental component of the EMF should be equal to or higher than that of the initial model to satisfy the required output power, even if the THD of the EMF and the cogging torque are reduced [16-18]. Therefore, the magnitude of the fundamental component is also included in the objective functions.

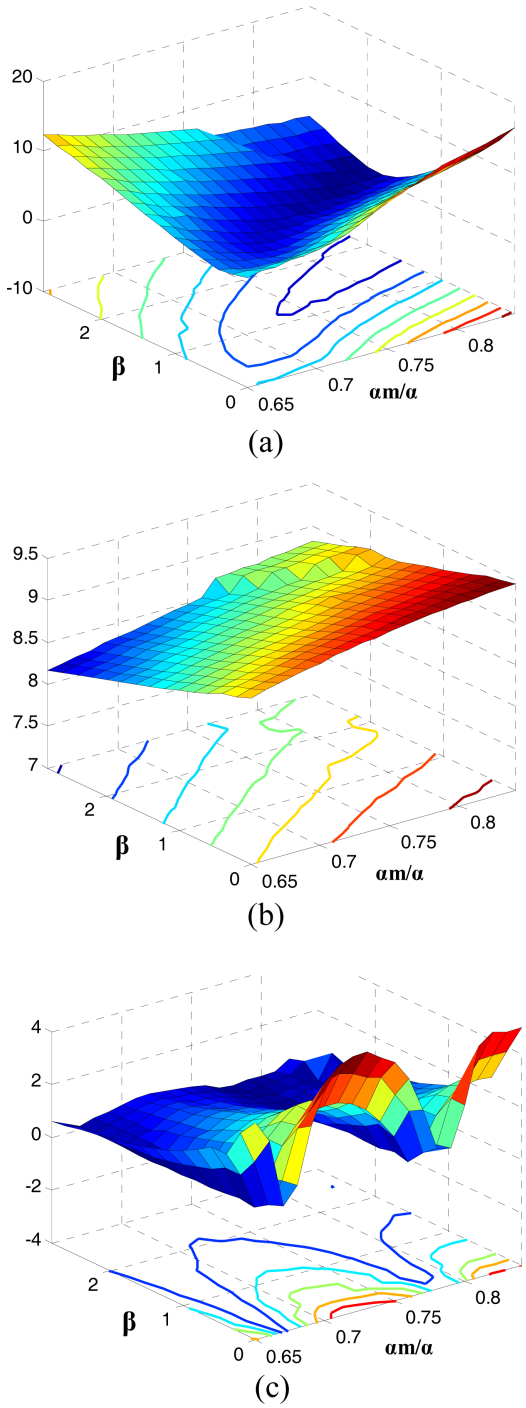

Fig. 4. (Color online) Calculation of the objective functions with respect to the design variables α_m/α and β. (a) THD of the phase EMF. (b) Fundamental components of the EMF. (c) Cogging torque.

Fig. 4 shows the THD of the phase EMF, the fundamental component of the EMF, and the cogging torque according to the two design variables. By changing α_m/α and β from 0.65 to 0.85 and from 0 to 3mm, respectively, each objective function is calculated and depicted in the figure. As α_m/α and β increase, the THD of the EMF decreases, as shown in Fig. 4(a). As α_m/α increases and as β decreases, the fundamental component of the EMF increases, as shown in Fig. 4(b). Therefore, the fundamental component of the EMF attains a maximum value at the point where α_m/α is a maximum, and β is a minimum. In Fig. 4(c), the cogging torque has the minimum value when α_m/α is 0.66-0.68 and 0.77-0.79. As β increases, the cogging torque decreases.

The ranges of the two design variables that minimize or maximize each objective function are determined. Finally, the optimal rotor shape is determined by choosing the design variables that satisfy all objective functions at the same time. Fig. 5 shows the improved rotor shape according to the optimal process, and the calculated THD of the EMF and the cogging torque are shown in Fig. 6. Both the THD of the EMF and the cogging torque are improved; particularly, the cogging torque is drastically reduced to 0.15 $Nm_{0\text{-}p}$ from 3.3 $Nm_{0\text{-}p}$. This is because the PM flux is dispersed onto the air gap surface with an increase in α_m/α, and the air gap flux density is transformed into a sinusoidal shape owing to the non-uniform air gap length by β.

2.3. Improved Model with q-Axis Flux Path (Final Model)

For the improved model, the THD of the EMF and the cogging torque are reduced compared to those of the initial model; however, the q-axis air gap length is increased owing to the increase in β. This causes a reduction in L_q,

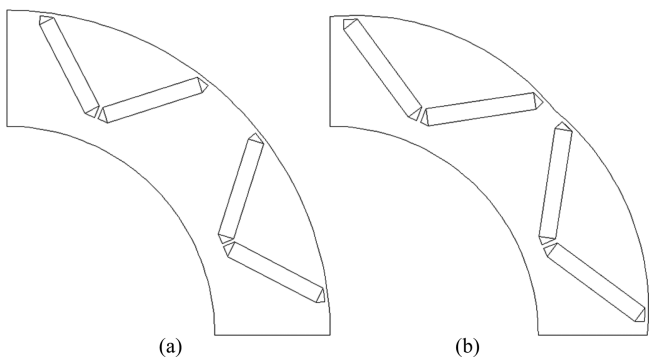

Fig. 5. Comparison of the rotor shape. (a) Initial model. (b) Improved model (model I).

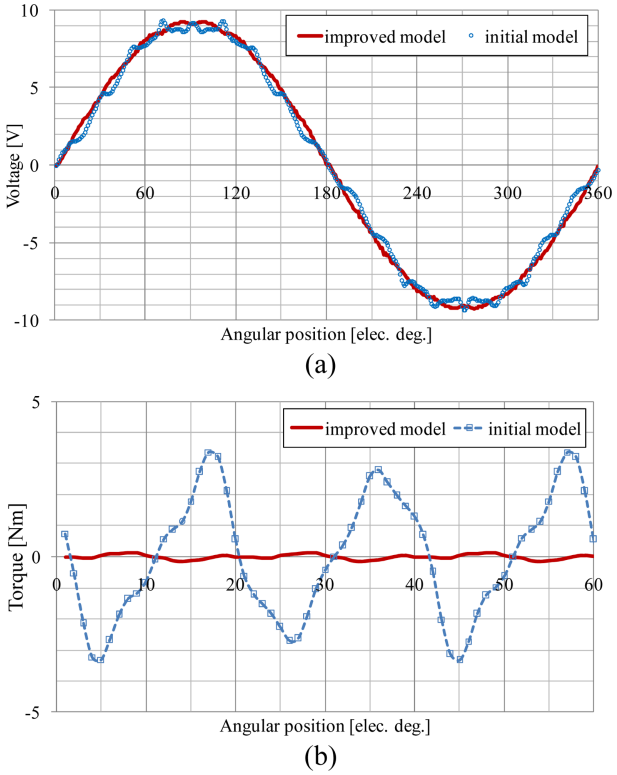

Fig. 6. (Color online) Comparison of the calculated results for the initial and improved models. (a) EMF waveform. (b) Cogging torque.

consequently decreasing the reluctance torque in proportion to the difference between L_q and L_d, as presented in (1). This causes a further reduction in the overall torque and efficiency. To address this problem, an additional flux path along the q-axis is proposed to increase the q-axis flux and inductance, as shown in Fig. 7. The q-axis air gap length is reduced by adding this flux path, which decreases the air gap reluctance. The reduced air gap reluctance decreases the total reluctance of the overall flux path, and the reduced total reluctance allows the flux

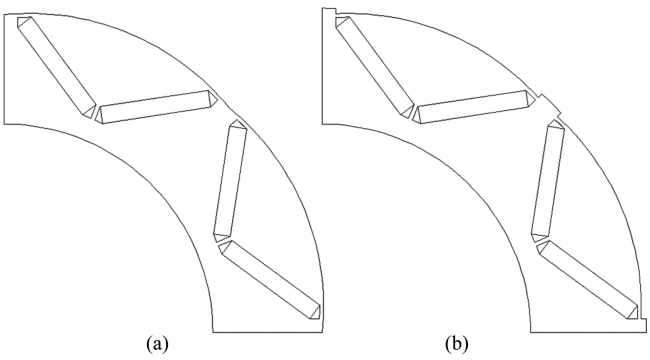

Fig. 7. Comparison of the rotor shape. (a) Improved model. (b) Improved model with a q-axis flux path (final model).

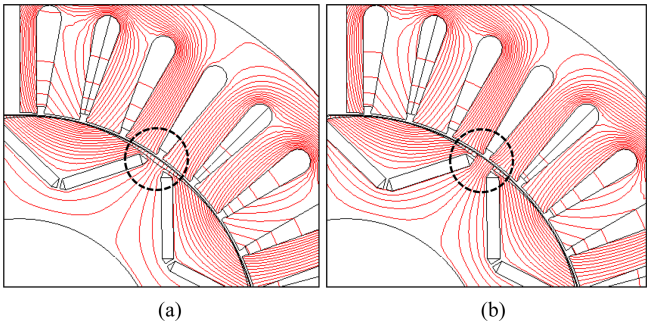

Fig. 8. (Color online) Comparison of the q-axis flux. (a) Improved model. (b) Final model.

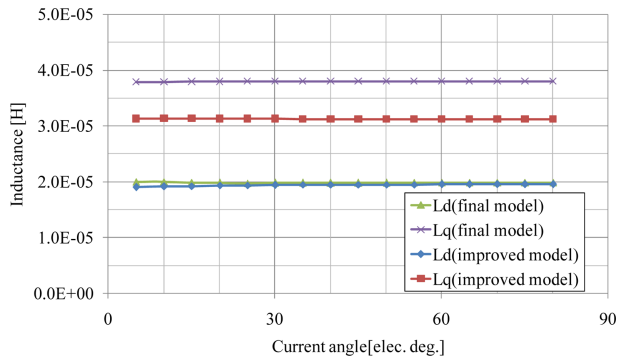

Fig. 9. (Color online) Comparison of the calculated d- and q-axis inductances for the improved and final models.

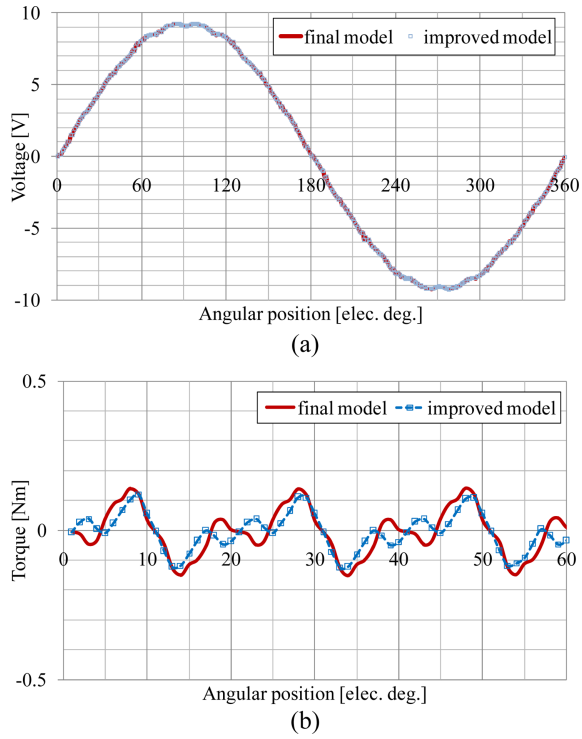

Fig. 10. (Color online) Comparison of the calculated results for the improved and final models. (a) EMF. (b) Cogging torque.

Table 2. THDs of the phase EMF and the Cogging Torques of the Three Models.

	THD of the EMF [%]	Cogging torque [Nm]
Initial model	6.1	3.3
Improved model	2.1	0.15
Final model	1.7	0.17

from the winding current to flow easily, which increases the flux linkage and inductance. This can be confirmed from the flux patterns of the q-axis currents in Fig. 8.

Fig. 9 shows the calculated L_d and L_q of the improved and final models. The additional flux path does not affect the d-axis flux; however, L_q is increased by 25% compared to that of the improved model. This increases the reluctance torque and consequently the total torque. The EMF and cogging torque of the two models are presented in Fig. 10. The results are almost the same because the additional flux path has little effect on the air gap flux density distribution, as for the d-axis flux. The THDs of the phase EMF and the cogging torques of the initial, improved, and final models are summarized in Table 2.

2.4. Torque Ripple and Iron Loss for Final Model

The torque ripples of the initial and final models are compared in Fig. 11. As expected, the torque ripple of the final model is reduced to 4.6% from 25.7% owing to the reduction in the THD of the EMF and the cogging torque.

The iron loss is calculated by [9, 10]

$$P_{iron} = k_{ed} f^2 B_{\max}^2 + k_{hys} f B_{\max}^2 , \quad (2)$$

$$\frac{P_{iron}}{f B_{\max}^2} = k_{ed} f + k_{hys} \quad (3)$$

where k_{ed} and k_{hys} are the eddy current and hysteresis loss constants, respectively; $B_{\max}$ is the maximum value of the magnetic flux density; and f is the frequency of the flux

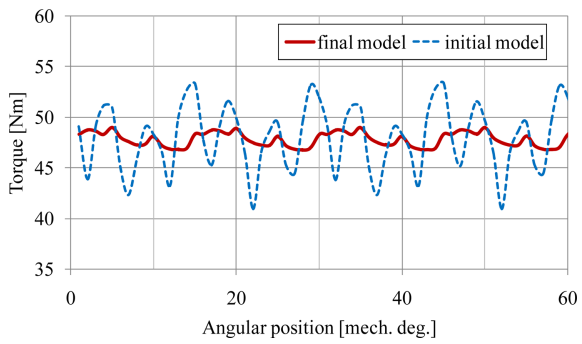

Fig. 11. (Color online) Comparison of the calculated torque ripples for the improved and final models.

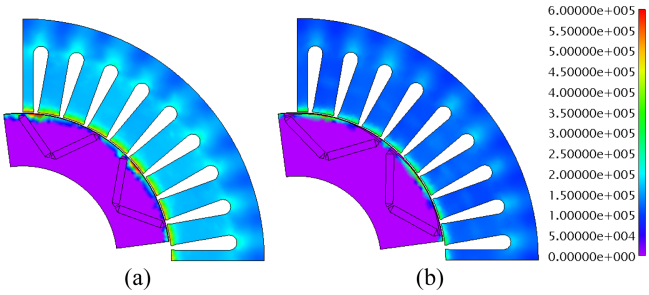

Fig. 12. (Color online) Comparison of the iron loss distribution at the rated load torque. (a) Initial model. (b) Final model.

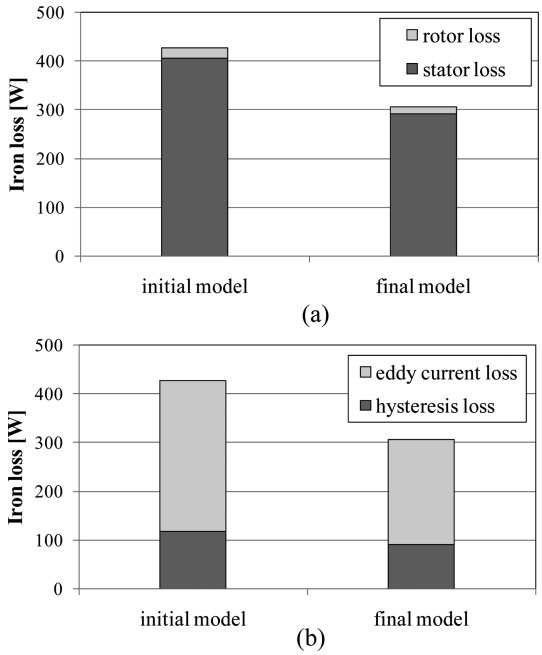

Fig. 13. Comparison of the calculated iron loss for the initial and final models. (a) Rotor and stator core losses. (b) Eddy current and hysteresis loss.

density. k_{ed} and k_{hys} are the experimental constant obtained by the Epstein frame. It means that (2) can be rewritten by (3) and the left side of (3) is a linear function with respect to the frequency f. Thus, k_{ed} and k_{hys} can be obtained from the slope and the intercept of the line of (3). The iron loss distributions and calculated values of the initial and final models are compared in Fig. 12 and Fig. 13. The iron loss for the stator core of the final model is reduced because the harmonics of the air gap flux density are reduced owing to the improved rotor design. The eddy current loss exhibits a larger decrease compared to the hysteresis loss because the eddy current loss is proportional to the square of the frequency, which is decreased by the reduction in the flux density harmonics.

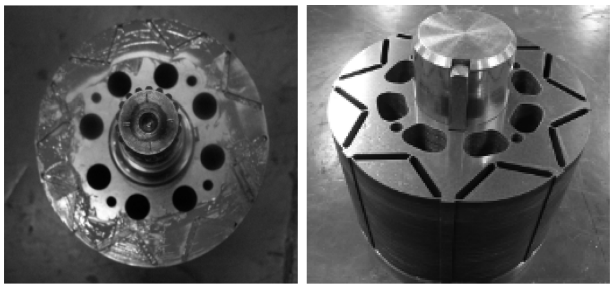

(a) (b)

Fig. 14. Manufactured rotor core. (a) Initial model. (b) Final model.

3. Manufacture and Verification of the Initial and Final Models

To verify the simulated results, prototypes of the initial and final models were manufactured and are shown in Fig. 14. The manufactured rotors were assembled on the same stator, and the EMFs for two models were measured for the same loading torque and speed. The measured EMFs and cogging torque are in good agreement with the calculated results in Fig. 2 and 10, as shown in Fig. 15 and 16.

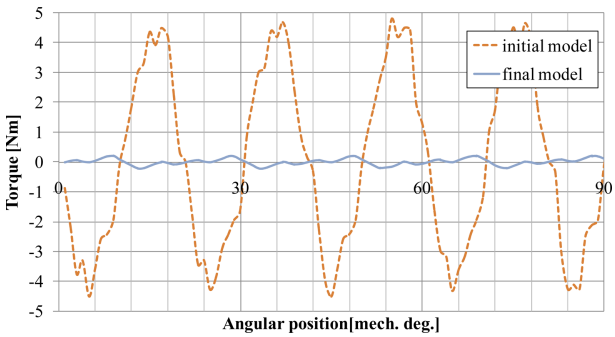

Fig. 16. (Color online) Measured cogging torque of initial and final models.

As shown in Fig. 17, the efficiencies of the two models at the rated power are similar to each other at 95%.

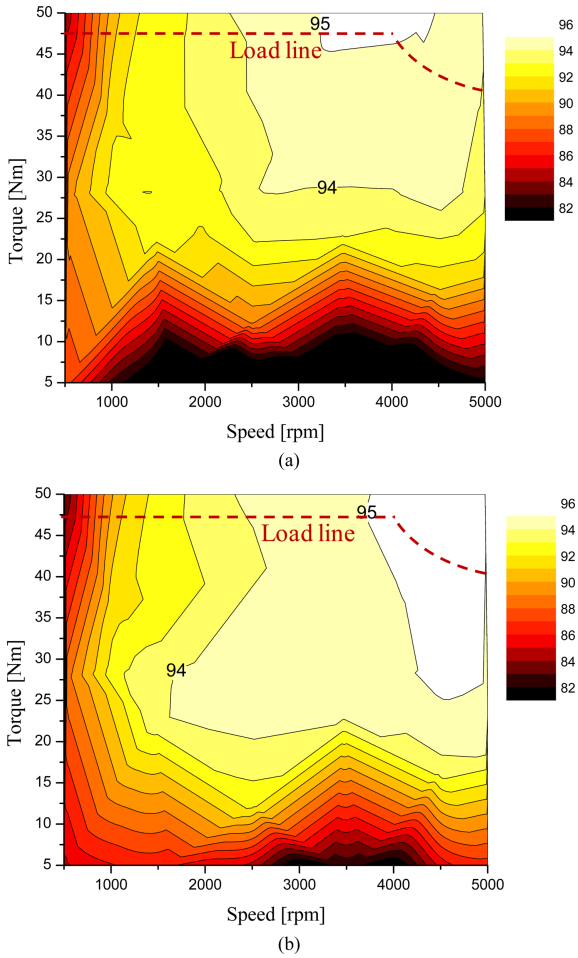

Fig. 17. (Color online) Comparison of the measured efficiency. (a) Initial model. (b) Final model.

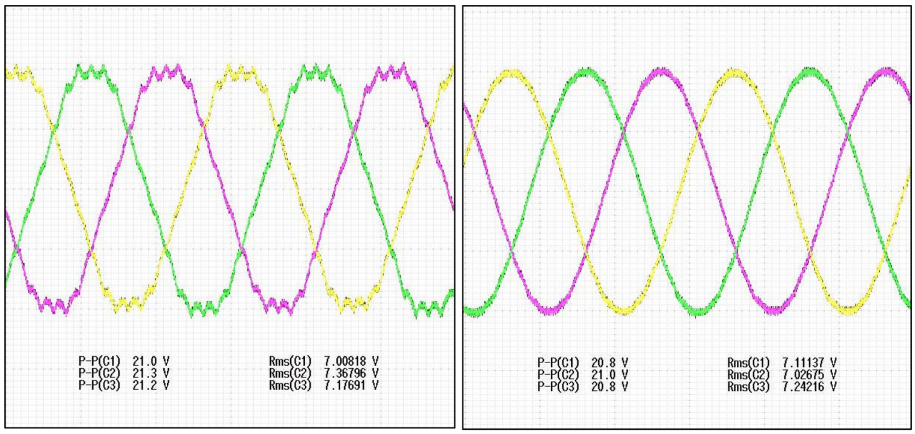

(a) (b)

Fig. 15. (Color online) Comparison of the measured EMF (5 ms/div and 5 V/div). (a) Initial model. (b) Final model.

However, the overall efficiency is increased for the final model. Furthermore, the driving region with a high efficiency is especially increased near the rated power. In addition, the final model has a higher efficiency in a constant-power region because the eddy current loss is decreased at a high speed. From the results, we confirm that the final model with an improved rotor shape is effective in terms of torque ripple and iron loss minimization.

4. Conclusion

We have developed a novel rotor shape for an IPMSM to decrease the torque ripple and iron loss by reducing the THD of the EMF and the cogging torque. An additional flux path along the q-axis was proposed and applied to the rotor to compensate for the reluctance torque that decreases owing to the improved shape.

The usefulness and feasibility of the proposed IPMSM and the validity of the analysis and design method were verified via experiment. This can help with the proliferation of the proposed motor, and it is the significant result of this study.

Acknowledgment

This work was supported by the Energy Efficiency & Resources of the Korea Institute of Energy Technology Evaluation and Planning (KETEP) grant funded by the Korea government Ministry of Knowledge Economy. (No. 20132010101870).

References

[1] Q. Weizhe, S. K. Panda, and J.-X. Xu, IEEE Trans. Power Electron. **19**, 272 (2004).
[2] R. Islam, I. Husain, A. Fardoun, and K. McLaughlin, IEEE Trans. Ind. Appl. **45**, 152 (2009).
[3] M. Ashabani and Y. A.-R. I. Mohamed, IEEE Trans. Magn. **47**, 795 (2011).
[4] Z. Azar, Z. Q. Zhu, and G. Ombach, IEEE Trans. Magn. **48**, 2650 (2012).
[5] W. Q. Chu and Z. Q. Zhu, IEEE Trans. Magn. **49**, 1211 (2013).
[6] T. W. Kim and J. H. Chang, J. Magn. **17**, 109 (2012).
[7] H. Domeki, Y. Ishihara, C. Kaido, Y. Kawase, S. Kitamura, T. Shimomura, N. Takahashi, T. Yamada, and K. Yamazaki, IEEE Trans. Magn. **40**, 794 (2004).
[8] D. Ionel, M. Popescu, C. Cossar, M. I. McGilp, A. Boglietti, and A. Cavagnino, Conf. Proc. IEEE IAS, 1 (2008).
[9] J.-H. Seo, T.-K. Chung, C.-G. Lee, S.-Y. Jung, and H.-K. Jung, IEEE Trans. Magn. **45**, 4656 (2009).
[10] J. W. Lim, Y. J. Kim, and S.-Y. Jung, J. Magn. **16**, 417 (2011).
[11] S. Morimoto, Y. Tong, and Y. Takeda, IEEE Trans. Ind. Electron. **41**, 511 (1999).
[12] J. Y. Lee, S. H. Lee, G. H. Lee, J. P. Hong, and J. Hur, IEEE Trans. Magn. **42**, 1303 (2006).
[13] T. Sun, J.-M. Kim, G.-H. Lee, J.-P. Hong, and M.-R. Choi, IEEE Trans. Magn. **47**, 1038 (2011).
[14] D. Braunisch, B. Ponick, and G. Bramerdorfer, IEEE Trans. Magn. **49**, 1407 (2013).
[15] F. Weizhong and P. C.-K. Luk, Conf. Proc. IEEE ECCE, 4998 (2013).
[16] Z. Wenxiang, C. Ming, H. Wei, J. Hongyun, and C. Ruiwu, IEEE Trans. Ind. Electron. **58**, 1926 (2011).
[17] A. Looser, T. Baumgartner, J. W. Kolar, and C. Zwyssig, IEEE Trans. Ind. Appl. **48**, 1258 (2012).
[18] D.-W. Kang, S.-C. Go, S.-H. Won, S.-B. Lim, and J. Lee, J. Magn. **15**, 36 (2010).